PNAS RESEARCH ARTICLE | EARTH, ATMOSPHERIC, AND PLANETARY SCIENCES

Isotopes illustrate vertical transport of anthropogenic Pb by reversible scavenging within Pacific Ocean particle veils

Nathan T. Lanning[a], Shuo Jiang[b,c], Vinicius J. Amaral[d], Katherine Mateos[d], Janelle M. Steffen[a], Phoebe J. Lam[d], Edward A. Boyle[b,1], and Jessica N. Fitzsimmons[a]

Contributed by Edward A. Boyle; received November 18, 2022; accepted April 27, 2023; reviewed by Luke Bridgestock and Christopher T. Hayes

Reversible scavenging, the oceanographic process by which dissolved metals exchange onto and off sinking particles and are thereby transported to deeper depths, has been well established for the metal thorium for decades. Reversible scavenging both deepens the elemental distribution of adsorptive elements and shortens their oceanic residence times in the ocean compared to nonadsorptive metals, and scavenging ultimately removes elements from the ocean via sedimentation. Thus, it is important to understand which metals undergo reversible scavenging and under what conditions. Recently, reversible scavenging has been invoked in global biogeochemical models of a range of metals including lead, iron, copper, and zinc to fit modeled data to observations of oceanic dissolved metal distributions. Nonetheless, the effects of reversible scavenging remain difficult to visualize in ocean sections of dissolved metals and to distinguish from other processes such as biological regeneration. Here, we show that particle-rich "veils" descending from high-productivity zones in the equatorial and North Pacific provide idealized illustrations of reversible scavenging of dissolved lead (Pb). A meridional section of dissolved Pb isotope ratios across the central Pacific shows that where particle concentrations are sufficiently high, such as within particle veils, vertical transport of anthropogenic surface–dissolved Pb isotope ratios toward the deep ocean is manifested as columnar isotope anomalies. Modeling of this effect shows that reversible scavenging within particle-rich waters allows anthropogenic Pb isotope ratios from the surface to penetrate ancient deep waters on timescales sufficiently rapid to overcome horizontal mixing of deep water Pb isotope ratios along abyssal isopycnals.

reversible scavenging | dissolved Pb isotopes | particle veils | Pacific ocean | GEOTRACES

Significance

Anthropogenic dissolved lead (dPb) isotope signatures can penetrate the entire water column bound to particles sinking from the upper ocean in certain portions of the Pacific Ocean. The process of reversible scavenging, the exchange of metals between solution and particles sinking down from the upper ocean, can explain how these anthropogenic isotope ratios can pervade the otherwise pristine deep ocean. Well established for other metals (thorium, protactinium, iron, zinc, copper, & nickel), reversible scavenging of Pb is less documented. This work shows that within "particle veils" in the North and equatorial Pacific, elevated particle concentrations support exchange between dPb and particles sufficiently rapidly to allow upper ocean anthropogenic Pb isotope signatures from the surface to reach the deep ocean.

Scavenging is the process by which dissolved metals adsorb onto the surfaces of particles. Scavenging of particle-reactive elements onto sinking particles has been long understood to be a major removal flux of metals from the ocean (1, 2). In 1982, Bacon & Anderson introduced the term "reversible scavenging," which is the process by which surface-active dissolved metals exchange onto and off of the surfaces of sinking particles, which effectively sustains metals in the dissolved phase but moves them to deeper depths in the water column (3–5). Bacon & Anderson (3) used the reversibility of scavenging to fit their models to their observed linearly-increasing concentration profile of the radionuclide ^{230}Th. Since then, reversible scavenging has been implicated for other elements with linearly-increasing profiles, such as copper (6). More recently, reversible scavenging has also been proffered to explain the decoupling of metals from each other [e.g., for Fe and Mn in hydrothermal plumes (7, 8) and from macronutrients (Cu, Zn, & Ni) (4–12)]. However, it remains difficult to differentiate reversible scavenging from subsurface biological regeneration, as both processes can move dissolved elements deeper into the water column. While models can help quantify these rates (6), isotopes are another diagnostic tool for diagnosing the influence of these element-deepening processes.

Lead (Pb) is an adsorptive element hypothesized to undergo scavenging, but not biological regeneration, and whose isotopes can help diagnose the presence of scavenging. Since preindustrial times, dissolved Pb (dPb) concentrations in the ocean have been strikingly altered by Pb emissions from industrial combustion processes, which carry Pb through the atmosphere to the surface ocean within aerosols (13–16). Collectively, these anthropogenic emissions supply more than ten times as much Pb to the oceans as natural (crustal) Pb fluxes and thus dominate the oceanic Pb cycle, emphasizing high Pb concentrations in surface waters (17–19). Although the phaseout of leaded gasoline in North America and Europe resulted in marked decreases in dPb of Atlantic Ocean surface waters over the last few decades (17), surface waters of the Pacific continue to be enriched by Pb-rich aerosols from Asian fossil fuel combustion (17, 20–22). Lead isotopes (e.g., ^{206}Pb/^{207}Pb and ^{208}Pb/^{206}Pb) are a useful tool for determining the origin of this pollutant,

Author contributions: N.T.L., P.J.L., E.A.B., and J.N.F. designed research; N.T.L., S.J., V.J.A., K.M., J.M.S., and P.J.L. performed research; N.T.L., P.J.L., E.A.B., and J.N.F. analyzed data; and N.T.L., P.J.L., E.A.B., and J.N.F. wrote the paper.

Reviewers: L.B., University of Cambridge; and C.T.H., University of Southern Mississippi.

The authors declare no competing interest.

[1]To whom correspondence may be addressed. Email: eaboyle@mit.edu.

This article contains supporting information online at https://www.pnas.org/lookup/suppl/doi:10.1073/pnas.2219688120/-/DCSupplemental.

Published May 30, 2023.

as Pb from different ore sources carries distinguishable isotope ratios (16, 21, 23, 24). For example, United States-sourced anthropogenic Pb has a $^{206}Pb/^{207}Pb$ 1.17 to 1.21 ($^{208}Pb/^{206}Pb$ ~2.10), while Chinese-sourced anthropogenic Pb has a $^{206}Pb/^{207}Pb$ = 1.14 to 1.18 ($^{208}Pb/^{206}Pb$ = 2.10 to 2.12) (16, 22, 24–26). Thus, Pb isotope ratios of North Pacific surface waters have been interpreted as a weighted measure of the relative flux of North American and Asian anthropogenic Pb (23, 25).

One feature of the oceanic Pb isotope distributions that has surprised oceanographers in the last decade is the discovery that anthropogenically sourced Chinese Pb isotopic signatures [$^{206}Pb/^{207}Pb$ = 1.14 to 1.18; $^{208}Pb/^{206}Pb$ = 2.1 to 2.12; (4, 25, 26)] can penetrate deep into abyssal waters of the Pacific Ocean (4, 18, 23). Since North Pacific deep waters have not ventilated in hundreds of years, we might instead expect the abyssal Pb in these waters to have preindustrial, crustal Pb isotope ratios ($^{206}Pb/^{207}Pb$ ~1.21) (4, 23). It was hypothesized that this deep ocean isotope anomaly is caused by reversible scavenging onto sinking particles, which carry Pb to otherwise pristine preindustrial abyssal waters (4). In the case of dPb, recent work has shown that in a particle-rich estuarine environment, dPb isotopes will reversibly exchange onto particles (27). Additionally, work in both the Pacific and Atlantic Oceans have invoked reversible scavenging to explain the transport of anthropogenic dPb from the surface to depth (4, 5).

While reversible scavenging should happen everywhere that an adsorptive element is present, its impact on oceanographic distributions depends on several conditions, including the time-dependent spatial gradients of Pb concentrations, the surface-deep gradient in isotope ratios, the vertical particle flux carrying the sinking particles deeper, and the horizontal mixing rates that might serve to dilute any dissolved metal flux to deeper waters. Thus, it is important to study the limits of these controlling factors to predict where reversible scavenging might be an important process. Particle veils, which are narrow regional bands of high particle flux (28), present a unique opportunity to study the impact of reversible exchange observed on dPb isotopes because they contrast high- and low-particle flux conditions over a small spatial scale of otherwise similar gradients of Pb concentrations, Pb isotope ratios, and horizontal transport regimes.

In this study, we present a meridional view of the central Pacific Ocean that crosses two particle veils: one at the equator and another at the subtropical–subarctic transition zone (~30 to 45°N). The equatorial veil is well documented to be a narrow band of high particle flux associated with the upwelling-driven equatorial phytoplankton bloom (28). In contrast, to the veil observed in the North Pacific is much wider and migrates seasonally with the "Transition Zone Chlorophyll Front" (TZCF) that forms at the boundary between the subtropical and subarctic gyres (29, 30) (Fig. 1). Here, we aim to demonstrate how reversible scavenging is a particularly powerful transporter of anthropogenic dPb isotopic signals from the surface ocean into deep waters within these particle veils. We implement a reversible scavenging model that highlights which factors control the magnitude of the isotope anomaly and depth to which the anomaly is deepened. This meridional snapshot illustrates how reversible scavenging can variably influence trace element and their isotope distributions on basin scales.

Results & Discussion

In 2018, the U.S. GEOTRACES program conducted the Pacific Meridional Transect (GP15), a full-depth water column assessment of trace elements and their isotopes from the Alaskan coast

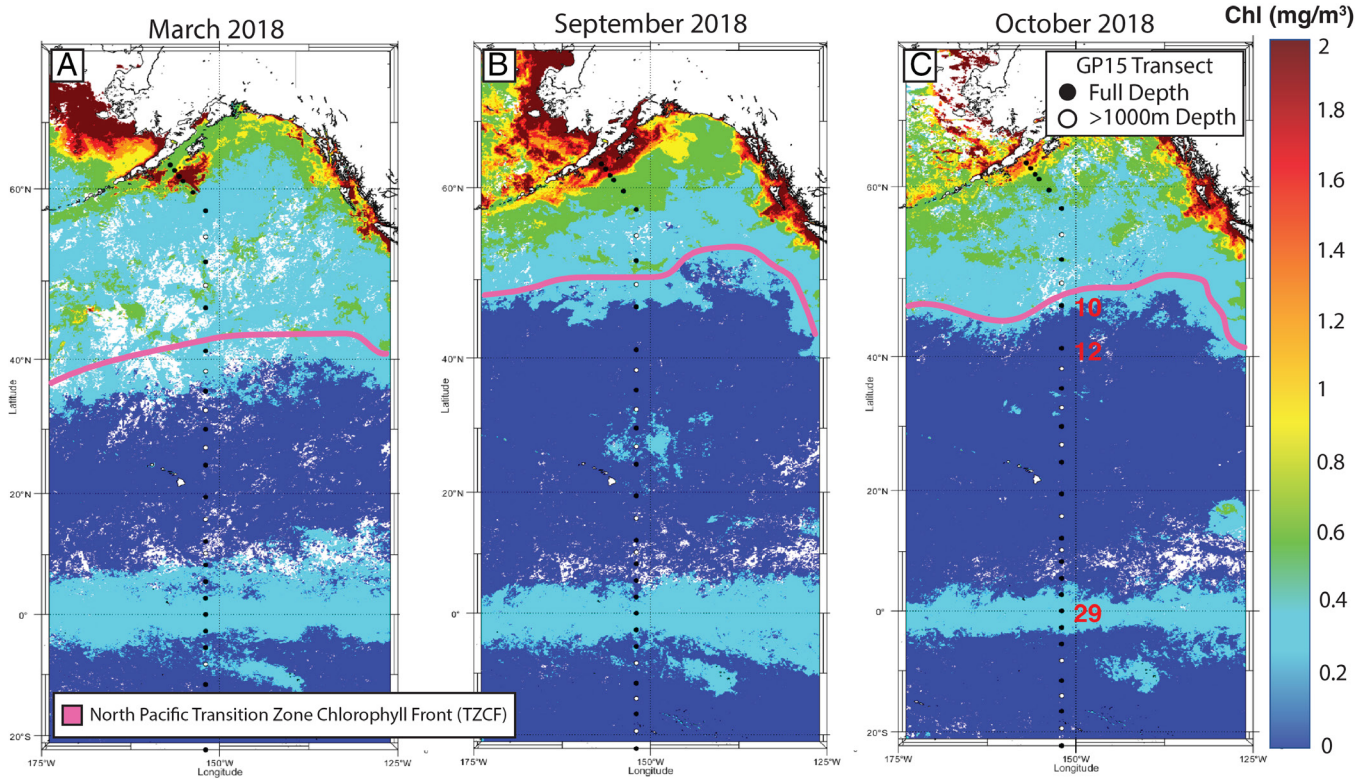

Fig. 1. Surface chlorophyll data from the National Aeronautics and Space Administration (NASA) Aqua MODerate resolution Imaging Spectroradiometer (MODIS) satellite for (*A*) a spring end member such as March 2018, (*B*) a fall end member such as September 2018, and (*C*) the month of the GP15 cruise, October 2018. The pink line highlights the transition zone chlorophyll front (TZCF) at 0.2 mg/m^3 in the North Pacific. U.S. GEOTRACES GP15 station markers are shown on each of the three panels, with the Panel *C* showing the labels in red for the prioritized stations of this paper: GP15 Stations 10 and 12 (TZCF) and 29 (Equator). Black dots represent stations where samples were collected from the entire water column, while white dots represent stations where samples were collected from the upper 1,000 m only.

southward to Tahiti along the 152°W meridian (Fig. 1). This transect is the most detailed sampling of dissolved Pb (dPb) and its isotopes ($^{206}Pb/^{207}Pb$ and $^{208}Pb/^{206}Pb$) in the central Pacific Ocean to date, allowing us the opportunity to assess the role of reversible scavenging on dPb isotopes within particle veils. We focus here on the dPb concentration and isotope ratio dynamics within the particle veils, while a future paper will more completely review Pb cycling along the full section.

Lead concentrations in the North Pacific are dominated by a subsurface plume (<2,000 m deep) extending as far north as the Alaskan slope and extending southward to ~3°N (Fig. 2*A*). It is well documented that the North Pacific is presently influenced by Asian dust contaminated with industrially produced Pb, which is carried eastward through the North Pacific Intermediate Water (NPIW) water mass and North Pacific Mode Waters (4, 16, 31, 32). Subsurface dPb enrichments exceed 60 pmol/kg, which is in stark contrast to deep Pacific waters that have not ventilated in hundreds of years and thus exhibit much lower, more "pristine" concentrations ranging from 1 to 2 pmol/kg in the abyssal South Pacific and 3 to 7 pmol/kg in the North Pacific. The distribution of dPb isotopes (reported here as $^{206}Pb/^{207}Pb$ and $^{208}Pb/^{206}Pb$) in intermediate waters boasts a signature of 1.16 to 1.17 ($^{206}Pb/^{207}Pb$; Fig. 2*D*) and 2.10 to 2.12 ($^{208}Pb/^{206}Pb$; Fig. 2*E*), which confirms a Chinese-dominated anthropogenic source of this abundant subsurface dPb.

However, the Pacific sections of $^{206}Pb/^{207}Pb$ (Fig. 2*D*) and $^{208}Pb/^{206}Pb$ (Fig. 2*E*) are not characterized by an intermediate water plume of the same shape as the dPb concentrations but are instead dominated by two distinct full-water column anomalies: 1) in the North Pacific identified at GP15 stations 10 (42°N) and 12 (37°N), and 2) at the equator sampled at GP15 station 29 (0°). These are the exact locations of known particle veils in the Pacific Ocean, identifiable by high total particulate inorganic carbon (PIC) concentrations (30); Fig. 2*F*), high total particulate suspended particulate matter concentrations (SPM; Fig. 2*C*), elevated surface chlorophyll concentrations (Fig. 1), as well as low total ^{234}Th activity at the surface, suggesting high particle flux (33). The contrast in dPb isotope ratios at these stations is striking, and their penetration to the seafloor confirms that some amount of dPb, with the isotopic signal of subsurface-enriched dPb, must be transported into deep waters of the Pacific (4).

The currently accepted mechanism responsible for transport of anthropogenic dPb to the abyss is reversible exchange of dPb via sinking particles. The first evidence for reversible scavenging of oceanic Pb (5) came from the western North Atlantic Ocean near Bermuda and showed a similarity of dPb concentration and pPb isotope ratio profiles that conform to the behavior of the reversible exchange models of Bacon & Anderson. This study concluded that suspended particles could reach isotopic equilibrium sufficiently faster than their residence time within a given depth range, suggesting that subsurface anthropogenic dPb could be transported deeper into the North Atlantic. The effect of reversible isotope exchange was modeled in the North Pacific years later in an attempt to identify a mechanism for why deep ocean dPb isotope ratios were shifted toward more anthropogenic values and away from preindustrial crustal signatures in a region that does not experience proximal deep-water formation (4). The authors determined, using field data collected in 2004 to 2005 implemented

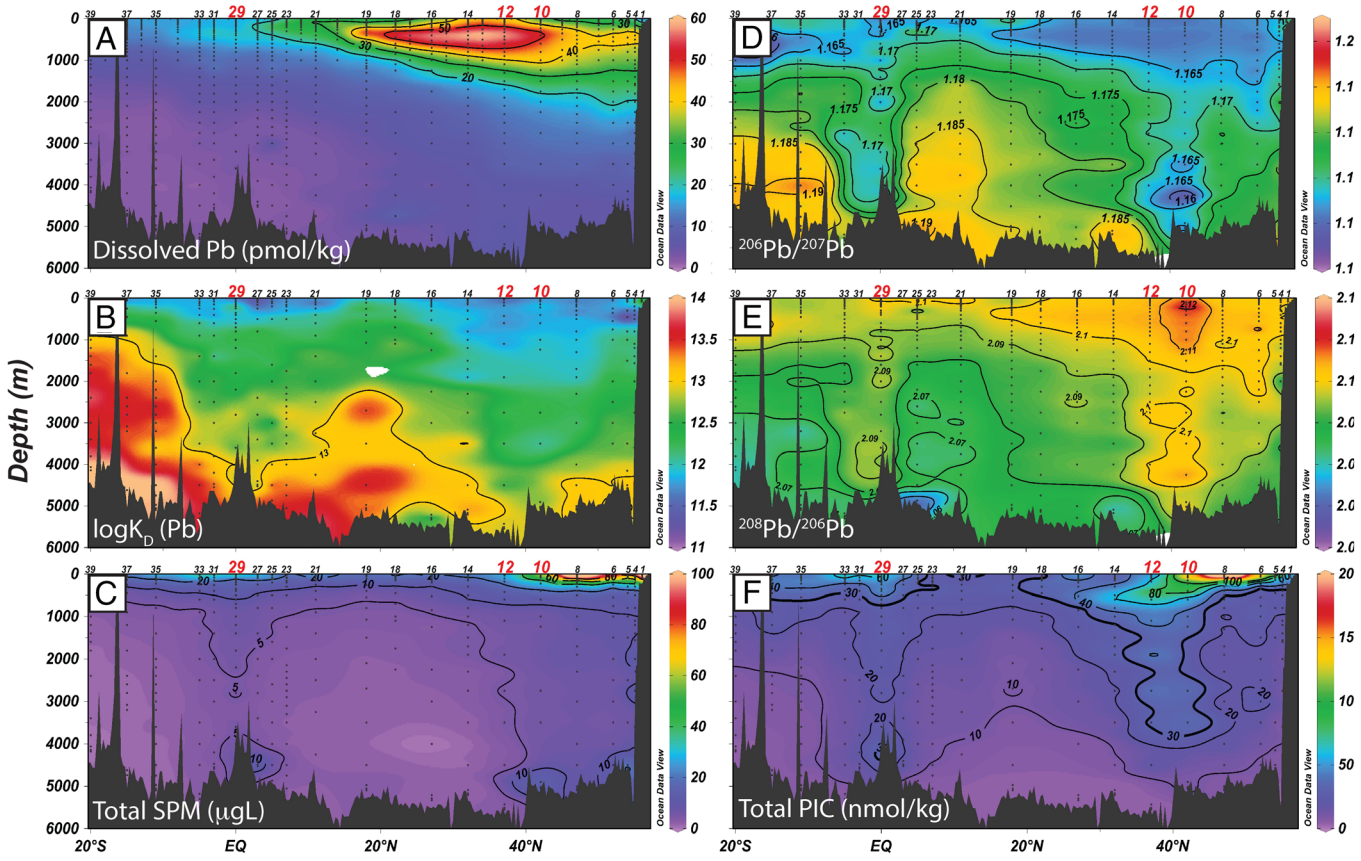

Fig. 2. Section plots of (*A*) dissolved Pb (pmol/kg), (*B*) logK$_D$ of Pb, (*C*) total suspended particulate matter (SPM; µg/L), (*D*) dissolved $^{206}Pb/^{207}Pb$, (*E*) dissolved $^{208}Pb/^{206}Pb$, and (*F*) total particulate inorganic carbon (PIC; nmol/kg from Bishop et al., 30) across the U.S. GEOTRACES Pacific Meridional Transect (GP15) along the 152°W meridian. Stations of interest within particle-rich veils are labeled in red (Stations 10, 12, and 29).

into a 1-D box model, that particles will scavenge dPb from surface seawater, transport that dPb to depth, and remobilize the dPb by reequilibrating with deep seawater isotopes. This finding implies that the concentration of abyssal dPb has increased in the North Pacific by ~2.4 pM due to reversible scavenging, a small absolute concentration but a large relative concentration increase for these Pb-poor deep waters. These papers and others conclude that anthropogenic aerosols and reversible scavenging are the primary source of dPb to the deep North Pacific, with expectations that the dPb concentration has risen even more substantially over subsequent decades (4, 19, 23, 31).

However, this GP15 dPb isotope section is the first dataset of sufficient size and basin-scale coverage to identify the conditions under which these anomalous dPb isotope "columns" can penetrate deep waters, such that we can anticipate where we may expect to observe similar columns within other ocean basins. To help identify the role that particles play in these columnar features, the adsorption distribution coefficient (K_D; dimensionless), which assesses the partitioning of an element between the particulate and dissolved phases, was calculated across the transect (Fig. 2*B*) using the following equation previously utilized for Th and repurposed for Pb (34):

$$K_D(\mathrm{Pb}) = \frac{pPb\,(pmol)\,/\,SPM\,(g)}{dPb\,(pmol)\,/\,Solution\,(g)} = \left(\frac{labile\,pPb\left(\frac{pmol}{m^3}\right)}{dPb\left(\frac{pmol}{m^3}\right)}\right) \times \left(\frac{1}{SPM\left(\frac{g}{g}\right)}\right). \quad [1]$$

In this study, we have used the "labile" (weak-acid leachable) particulate Pb (pPb) concentrations to focus on the exchangeable portion of pPb. Both labile pPb and SPM concentrations are from the small (1 to 51 μm) particulate size fraction (*Methods*). Small particles defined this way account for ~80% of the total particle mass (35) and have an even greater portion of the particle surface area available for adsorption, and thus play an important role in the reversible scavenging and transport of anthropogenic isotopes to depth.

The resulting K_D distribution, shown as logK_D in Fig. 2*B*, shows low values in the upper water column where SPM is high, with generally higher values at depth where SPM is low. An inverse relationship between K_D and SPM has been identified in the past, termed the particle concentration effect (36, 37), and may be the dominant control on the K_D distribution in this section (38). The low K_D values extend all the way to the bottom most clearly at the particle-rich veils (Stns 10, 12, & 29), mirroring the elevated SPM in those regions. The deep anomalies in the $^{206}Pb/^{207}Pb$ and $^{208}Pb/^{206}Pb$ ratios generally also occur in these same regions of high SPM and low K_D, but with a more prominent "columnar effect" at Station 29 at the equator and Stations 10 and 12 in the North Pacific than either of the aforementioned K_D or SPM concentrations.

Large numbers of sinking particles will allow the most surface-active dPb from seawater to adsorb to particles in the upper ocean and be transported down to the abyss where the Pb can exchange back into the dissolved phase. Thus, particle-rich veils should more efficiently transport anthropogenic surface dPb signals to the deep than regions with low particle fluxes. To test this idea, we constructed a simple box model (Fig. 3) that can account for the vertical dPb isotope signals in particle veil regions based off a 1-D model constructed by Wu et al. (4). They proposed that Pb is transported from the upper Pacific Ocean into the deep by reversible exchange with sinking particles. As the anthropogenic flux accumulates with a distinctly different isotope composition ($^{206}Pb/^{207}Pb$ ~1.188) than that of the previous crustal steady-state ($^{206}Pb/^{207}Pb$ ~1.21), a fraction of the Pb adsorbs to the particles, sinks, and then is released back into the lower dPb concentration deep water according to a reversible K_D distribution coefficient (4). This scenario envisages a century-scale evolution that continues from the past into the near future.

The premise of our particle veil model is that the sinking flux of distinct dPb isotope ratios from the upper ocean is sufficient to alter the dPb isotope ratios at the bottom of the deep veil "box," despite the tendency of isopycnal eddy diffusion (K_H) to eliminate horizontal gradients. Consider a narrow deep box bounded by, effectively, infinite reservoirs of pristine abyssal Pb to the north and south (Fig. 3*A*). We calculate how a latitudinally narrow ($\boldsymbol{w}$ ~ 500 km), longitudinally wide ($\boldsymbol{l}$ ~ 5,000 km), deep ocean box ($\boldsymbol{h}$ ~ 2 km) is affected by an enhanced sinking flux of reversibly exchangeable Pb from above. If there was no flux from above, lateral mixing would cause the veil box to have the imposed boundary conditions from the exterior deep reservoir box. Consequently, regions outside of the particle veil box would not display any unique $^{206}Pb/^{207}Pb$ or $^{208}Pb/^{206}Pb$ isotopic fingerprint throughout the water column because of reversible isotopic exchange. We assume that particles start off in K_D equilibrium with intermediate water (~1,000 m) at the top of the box, then exchange within the deep box, and finally leave the box at the bottom (3,000 m) with a new isotopic composition. The observed isotopic composition resulting from that vertical flux is attenuated by lateral diffusion bringing in nonveil Pb isotope ratios from neighboring deep ocean boxes. To clarify, advective fluxes along this transect were considered to be minor and are thus ignored. The equation below outlines the calculations made for this model (variables defined in Fig. 3*B*):

$$0 = \frac{d[Pb]}{dt} = \frac{1}{lwh}\left[S\Delta l\Delta w\left\{[pPb]_{1000} - [pPb]\right\} - \frac{2\Delta l\Delta h K_H}{\Delta w}\left\{[dPb] - [dPb]_{outside}\right\}\right]. \quad [2]$$

In our calculation, each Pb stable isotope concentration (^{206}Pb, ^{207}Pb, and ^{208}Pb) is treated separately, and the isotope ratios are calculated from the individual isotope concentrations: the dissolved and pPb concentrations at the top of the veil box ($[dPb]_{1000}$, $[pPb]_{1000}$, respectively), the total particulate concentration at the top of the veil box (P_{tot}), the dPb concentration in the deep ocean outside of the veil ($[dPb]_{outside}$). The box concentrations are taken from the observed dissolved and particulate concentrations for each station. K_D is calculated from Eq. **1** using the ratio of particulate to dissolved lead at the top of the veil box in reference to small particulate SPM. The sinking rate (S) is chosen to be consistent with ^{230}Th-based estimates for "bulk" particle residence times calculated across previous GEOTRACES transects (39). The value of the K_H was obtained from ARGO-based estimates (40) (Fig. 3*B*). *SI Appendix*, Table S1 contains all parameters utilized in our model, with their associated symbols.

The model was applied to the equatorial and transition zone particle veils separately (Fig. 3*B*). In the North Pacific, the model results predicted a small increase in dPb concentration (0.6 pmol/kg) with a noticeable shift in dissolved $^{206}Pb/^{207}Pb$ and $^{208}Pb/^{206}Pb$ in the deep particle veil box toward more anthropogenic values ($^{206}Pb/^{207}Pb$ = 1.174; $^{208}Pb/^{206}Pb$ = 2.087; Fig. 3*B*). This is consistent with the observed values from Stations 10 to 12 between 2,000 and 4,000 m depth ($^{206}Pb/^{207}Pb$ = 1.16 to 1.175; $^{208}Pb/^{206}Pb$ = 2.09

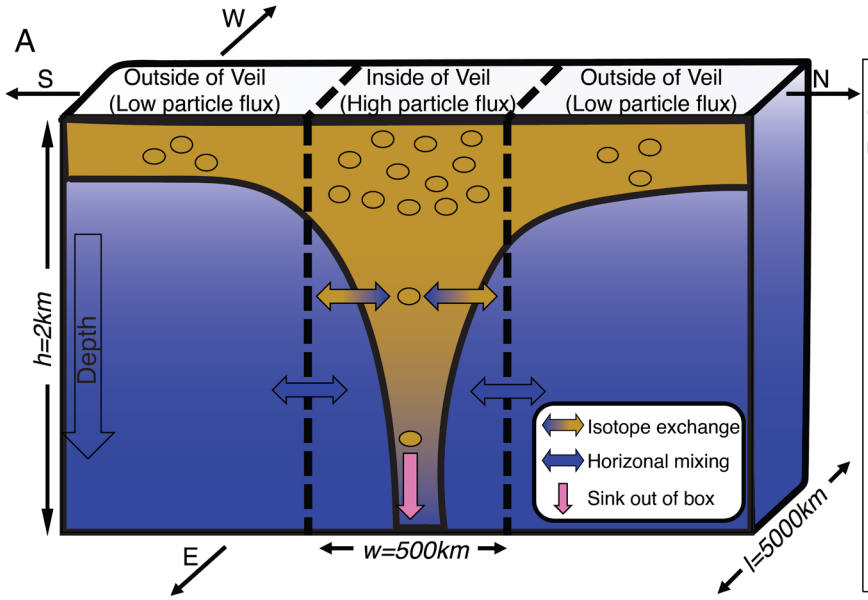

B

Variable	North Pacific	Equator
dPb at 1000m in box [dPb]$_{1000}$ (pmol/kg)	41.5	16.4
pPb at 1000m in box [pPb]$_{1000}$ (pmol/kg)	0.3	1.0
dPb outside deep box [dPb]$_{outside}$ (pmol/kg)	11.4	5.7
Total pPb at top of box (P_{tot}; g/m^3)	6.E-03	7.E-03
Latitudinal width of box (*w*; km)	500	500
Longitudinal length of box (*l*; km)	5000	5000
Vertical height of box (*h;* km)	2	2
^{206}Pb/^{207}Pb just above veil box	1.162	1.161
^{208}Pb/^{206}Pb just above veil box	2.111	2.094
^{206}Pb/^{207}Pb outside of veil box	1.177	1.181
^{208}Pb/^{206}Pb outside of veil box	2.087	2.075
Sinking Rate (S; m^2/yr)	500	500
Horizontal Advection (K_H; m^2/sec)	300	300
Distribution Coefficient (K_D)	9.83E+05	1.60E+0

C

Variable	North Pacific			Equator		
	Model	Observed	Difference	Model	Observed	Difference
[dPb] in the deep veil box (pmol/kg)	12.0	11.4	5.14%	2.6	2.9	8.15%
[pPb] in the deep veil box (pmol/kg)	0.07	0.10	30.5%	0.03	0.05	61.4%
^{206}Pb/^{207}Pb in the deep veil box	1.174	1.166	6.62‰	1.173	1.170	2.58‰
^{208}Pb/^{206}Pb in the deep veil box	2.087	2.106	8.87‰	2.089	2.088	0.57‰

Fig. 3. A box model was constructed to calculate the transport of anthropogenically influenced dPb concentrations and isotope signals from intermediate waters down into the deep water column of particle-rich veils. (*A*) Visual representation of the model with the particle veil depicting heightened particle flux from the upper water column compared to outside of veil regions. The model domain is a deep ocean box between 1,000 m depth at the *Top* and 3,000 m depth at the *Bottom*. The brown dots represent particles that isotopically exchange with ambient seawater-dissolved ^{206}Pb/^{207}Pb and ^{208}Pb/^{206}Pb of anthropogenic origin in the upper 1,000 m and transport the anthropogenic signal into the deep box indicated by the brown to blue vertical gradient plume. In the box, some of the particulate Pb isotopically exchanges back off into ambient seawater (brown/blue gradient arrows), overwhelming the influence of horizontal mixing at depth by supplying preindustrial, natural dPb isotope signals (blue arrows). The particle will eventually sink out of the bottom of the box (3,000 m) shown by the pink arrow. (*B*) Table of variables used in the box model with assumed parameters colored in black. Variable descriptions are as follows: estimated particle sinking rate (S), horizontal eddy diffusion (K_H), dPb at the top of the box ([dPb]$_{1000}$), particulate Pb at the top of the box ([pPb]$_{1000}$), total particulate concentration at the top of the box (P_{tot}), box width (*w*), box length (*l*), box height (*h*), dPb in the deep ocean outside of the veils ([dPb]$_{outside}$), adsorption distribution coefficient (K_D), dPb at the bottom of the veil box ([dPb]), particulate Pb at the bottom of the veil box ([pPb]; *SI Appendix*, Table S1). (*C*) Table of model results and field observations, with percent difference (% Difference) indicated to compare our model output to observed data.

to 2.10; Fig. 2 *D* and *E*). Calculated percent differences between the deep box model data and field observations indicated that the model well predicted dPb concentrations (5.14% difference), ^{206}Pb/^{207}Pb (6.62‰), and ^{208}Pb/^{206}Pb (8.87‰) but underpredicted pPb concentrations (30.5%) (Fig. 3*C*).

The equator model showed slightly different results. Due to the depleted concentrations of dPb in the surface equatorial Pacific compared to the North (Fig. 2*A*), the reversible scavenging flux of dPb to depth was diminished, resulting in no substantial modeled increase in dPb concentration in the deep particle veil box but rather a decrease (3.2 pmol/kg) compared to outside the veil, matching well with field measurements (8.15% difference; Fig. 3*C*). As in the North Pacific, pPb concentrations were underestimated in our box model (61.4% difference), again exaggerated by the low pPb concentrations observed at the Equator (pPb = 0.5 pmol/kg). Regardless of changes in dPb concentration, both dPb isotopic ratios once again shifted toward more anthropogenic values (^{206}Pb/^{207}Pb = 1.173; ^{208}Pb/^{206}Pb = 2.089; Fig. 3*B*), in strong agreement with dPb isotope observations in deep waters of Station 29 (^{206}Pb/^{207}Pb = 1.165 to 1.175; ^{208}Pb/^{206}Pb = 2.08 to 2.10; so 2.58‰ and 0.57‰ difference, respectively, Fig. 2 *D* and *E*).

The GP15 observations show that deep waters of the North Pacific particle veil support slightly more anthropogenic dPb isotope ratios compared to the deep waters of the equatorial particle veil, consistent with a higher concentration anthropogenic dPb signal in NPIWs than that at the equator. However, the model somewhat surprisingly calculated similarly anthropogenic-influenced isotopic signature in deep waters of both particle veils. While the total particle concentration, sinking rate, and horizontal eddy diffusivity were the same or nearly the same at the equator and North Pacific in the model, the observed Pb concentrations and thus K_D values were different across the two veils: the upper water column dPb concentrations were more than twice as high in the North Pacific veil (Stn 10 & 12 had dPb of 55 to 62 pmol/kg) than those at the equatorial veil (Stn 29 max dPb of 20 pmol/kg). The same was true for the deep ocean dPb concentrations, which were higher in the North Pacific (>10 pmol/kg) than those at the equator (~5 pmol/kg). Despite these concentration gradients, the two particle veils still were predicted to have similar dPb isotopic ratios throughout the deep-water column. This makes sense, as it is easier for particle veils in regions of lower dPb concentrations to influence the isotopic composition of the dPb more easily throughout the water column. Overall, using values collected from the GP15 transect, the model results compare reasonably well to actual data sampled from inside each particle veil (Fig. 3*B*).

Compared to particle veil regions in which local upwelling supplies subsurface nutrients to fertilize surface primary production, Pacific waters outside of the particle-rich veils have diminished

upper ocean particle concentrations. A schematic of the controls on this $^{206}Pb/^{207}Pb$ reversible exchange is shown in Fig. 4. Since the central Pacific Ocean is dominated by low $^{206}Pb/^{207}Pb$ (Fig. 2*D*) in the intermediate layer, all particles, regardless of high or low particle flux, will exchange with this low $^{206}Pb/^{207}Pb$ signal. However, outside of the particle veils, there are insufficient particles available to transport the low $^{206}Pb/^{207}Pb$ signal to the abyss (Fig. 4*B*). Instead, in these areas, horizontal mixing of high $^{206}Pb/^{207}Pb$ from neighboring stations overwhelms that low $^{206}Pb/^{207}Pb$ reversibly released from the particles and dilutes any anthropogenic signal carried deep with scavenging. This means that reversible scavenging of low $^{206}Pb/^{207}Pb$ within high particle flux regions will overwhelm the horizontal mixing signature, allowing a pronounced anthropogenic isotopic fingerprint to penetrate the full water column into the abyss. Although not pictured, this mechanism would work similarly for $^{208}Pb/^{206}Pb$, resulting in anthropogenic, high isotope values at the surface and preindustrial, low values at depth.

Thus, our box model supports the hypothesis that in high-flux particle veils, reversible Pb exchange between particles and ambient seawater in the intermediate layer occurs on a timescale fast enough to transport anthropogenic dPb isotope signatures from the upper ocean into the otherwise-pristine deep ocean before the sluggish deep ocean mixing of "crustal" isotope signatures can spread laterally through the North Pacific Ocean (4). This allows the "columnar" anthropogenic dPb isotope anomalies that we observed on GP15 to be sustained within particle veils, a unique demonstration of the effects of particle fluxes and reversible scavenging on oceanic Pb distributions. The model we have applied to these three regions shows that it is predominantly the magnitude of particle flux and sinking rate, in comparison to the observed lateral diffusivity in abyssal waters, that drives the observed vertical isotope anomaly.

Also required to observe an isotope anomaly from reversible scavenging is an isotope ratio gradient between surface and deep ocean waters, such that particle exchange can imprint a unique upper ocean isotope signature on the deep sea as an anomaly. Importantly, the vertically columnar reversible scavenging effect is difficult to see in dPb concentrations along GP15, which only increased ever so slightly (<10 pmol/kg) above background concentrations; instead, it was apparent only in isotope space, driven by the large dPb isotope gradient between anthropogenic-influenced intermediate waters and the more pristine, crustal-influenced deep waters below. As a result, this unique feature can be difficult to diagnose in other global ocean basins sampled by past GEOTRACES surveys. In the Indian Ocean, the GI04 dPb isotope distributions are consistent with the reversible scavenging model proposed here, with postindustrial $^{206}Pb/^{207}Pb$ (1.15 to 1.165) signatures penetrating deep waters only in the Arabian Sea, where particle fluxes are highest along the transect (13). In the North Atlantic, a transitional surface chlorophyll front fluctuates seasonally around 30 to 40°N, which we might expect to drive a dPb reversible exchange pattern much like the North Pacific (41); however, no large-scale transects have measured dPb isotopes in this region. The GEOTRACES GA01 (42) and GA03 (43) transects identified anthropogenic dPb isotope signals throughout the water column ($^{206}Pb/^{207}Pb$ = 1.18 to 1.19), indicating past North American and European inputs, but not within any well-defined latitudinal band across a particle veil. Additionally, the strong horizontal transports of Mediterranean and Antarctic Intermediate Water, North Atlantic Deep Water, and Circumpolar Deep Water diminish the impact of local particle transport. Reversible

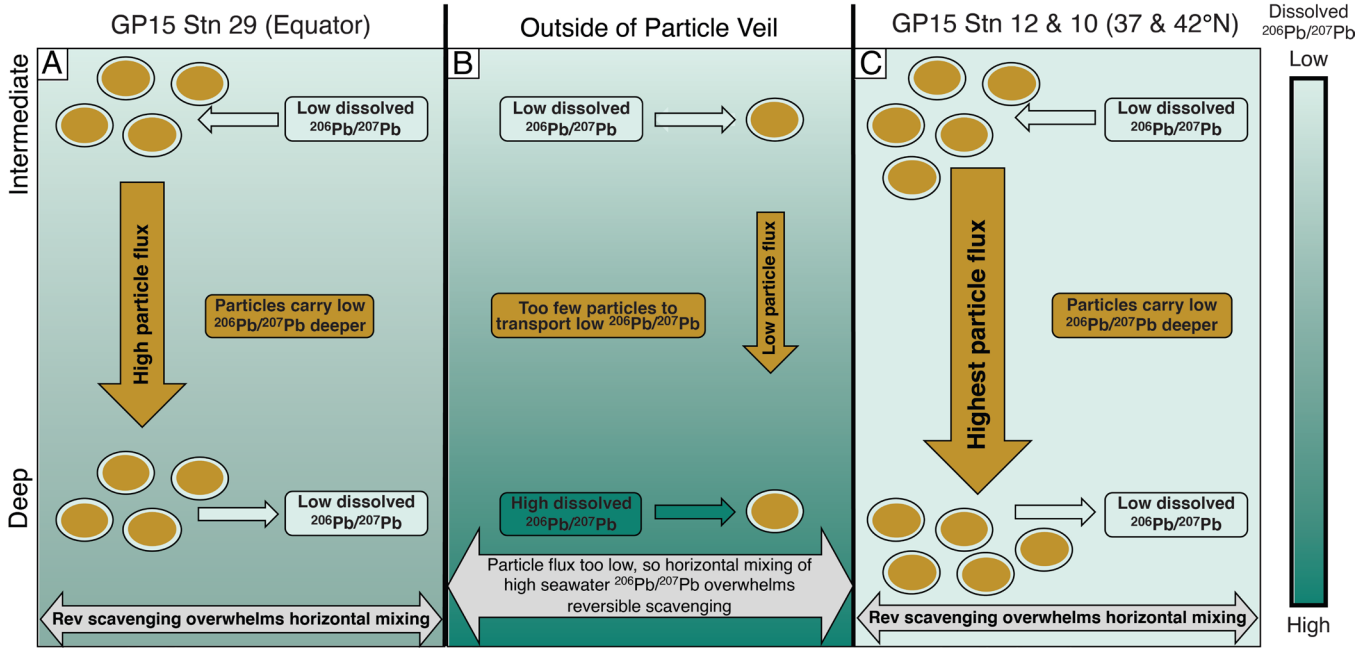

Fig. 4. Schematic of the role that reversible isotope exchange plays in Pb cycling within particle-rich veils at the (*A*) equator, compared to (B) outside of the particle veil and at the (*C*) subarctic–subtropical transition zone in the North Pacific 30 to 45°N. The background shading represents the ambient seawater-dissolved $^{206}Pb/^{207}Pb$ gradients inside and outside of particle veil regions. Brown ovals with a light-green outline represent particles transporting "low" ($^{206}Pb/^{207}Pb$ = 1.155 to 1.17), anthropogenically influenced dissolved $^{206}Pb/^{207}Pb$ signals from the intermediate layer (1,000 m) to the deep central Pacific. Low dissolved $^{206}Pb/^{207}Pb$ signatures will adsorb to all particles in the intermediate layer. Particle flux is represented by the number of particles in the intermediate layer as well as by the size of the vertical flux arrows. At the equator and in the North Pacific, the vertical particle flux is large enough for reversible scavenging of low $^{206}Pb/^{207}Pb$ signatures off particles to overwhelm the influence of "high" ($^{206}Pb/^{207}Pb$ = 1.19 to 1.21) dissolved $^{206}Pb/^{207}Pb$ that mixes horizontally into the region. In contrast, outside of the veils, the insufficient vertical particle flux does not reversibly scavenge enough low $^{206}Pb/^{207}Pb$ of anthropogenic origin to overwhelm the impact of horizontal mixing, leaving behind no anthropogenic imprint at depth.

scavenging of dPb onto particles has already been recorded near river mouths and margins (27), which further supports the hypothesis that high particle flux in areas of surface-deep isotope gradients is the primary control on the appearance of a reversible scavenging–derived isotope effect.

What types of marine particles facilitate reversible scavenging of Pb? Historically, it has been thought that Pb is preferentially scavenged onto manganese (Mn) oxide particles (44). Indeed, regions with higher Mn oxide particles in the Atlantic and Arctic Oceans had higher K_D for the radiogenic ^{210}Pb isotope (45, 46). But in order for the intermediate water anthropogenic Pb signal to be transferred to deep waters, it must also desorb from particles. Indeed, the dPb isotope anomalies appear in regions with relatively high SPM and low K_D. One possible interpretation for these columnar isotope effects, previously suggested to explain patterns in Th isotopes (38), is the increased presence of colloidal Pb that is supported within the dissolved phase and would therefore lower the K_D (38). This has been associated with the "particle concentration effect" which may be the dominant control on K_D. Higher particle concentrations mean more delivery of anthropogenic Pb to the deep ocean, and low K_D means that more of that Pb can be partitioned back to the dissolved phase in deep waters, potentially as colloids. This suggests that within these columnar features, colloidal pumping may force K_D to decrease while allowing an anthropogenic isotope signal to vertically penetrate throughout the deep ocean.

To test this, we compared the distribution of colloidal Pb (cPb; 0.003 to 0.2 μm) within the Equatorial particle veil at Stn 29 to that at Stn 19 (17.5°N), which is located outside of a particle veil. We utilized shipboard ultrafiltration to remove cPb from the dissolved phase, leaving the soluble (sPb; <0.003 μm~10 kDa) or "truly dissolved" size fraction remaining (47). Colloidal Pb ([cPb] = [dPb]–[sPb]) dominated the dissolved phase within the upper 1,800 m of the water column at Stn 29 (%cPb = [cPb]/[dPb]; <1,800 m %cPb = 46 to 84%), which had coincident low K_D values (*SI Appendix*, Fig. S2). In contrast, at Stn 19, which had high K_D values, there was minimal presence of cPb throughout the entire water column (*SI Appendix*, Fig. S2). These opposite cPb patterns in and out of the particle veils point to the possibility that colloidal pumping may help drive the low K_D values required to facilitate reversible scavenging in the Pacific particle veils. However, the coarse resolution of these cPb measurements prevents our excluding other explanations for the spatial variability in cPb concentrations observed, and thus we cannot conclusively attribute colloidal pumping to the K_D and reversible scavenging patterns without additional measurements.

Of all particle components, the dPb isotope anomalies are most similar to the distribution of total PIC (Fig. 2*F*), which is produced largely by coccolithophores that make up a large portion of the phytoplankton bloom at the North Pacific's TZCF (defined at a chlorophyll concentration of 0.2 mg/m^3) (29, 48). The nature of this potential association is not clear. As there is no evidence that PIC has any preferential scavenging capacity for Pb, this could imply a role for the influence of PIC on the sinking characteristics of particles (49). In fact, in the North Pacific, the penetration of anthropogenic dPb isotope signatures into deep waters is also present north of the TZCF at Stations 6 and 8 (45 to 52°N), just less deeply and less intensely than that in the active particle veil sampled at Stations 10 and 12 (35 to 45°N). The TZCF moves latitudinally throughout the year (Fig. 1 and *SI Appendix*, Fig. S1) (48, 50), ranging from 30°N in the spring (near Station 13) to 45°N in the summer (29, 51, 52). Importantly, the total SPM concentrations were also elevated (>5 μg/L) throughout the water column of the more northward Stations 6 and 8, in addition to the particle veils at Stations 10 and 12. Thus, it is the total SPM concentrations that appear to be the best tracer of dPb scavenging, not any one particle type in particular.

Importantly, the intermediate waters of these Stations 6, 8, 10, and 12 all contain dPb with the anthropogenic isotope fingerprints needed to distinguish the columnar effect of reversible scavenging from the deep water dPb isotope ratios. In contrast, Stations 14, 16, and 18 (20 to 35°N) have the anthropogenic dPb isotope ratios in intermediate waters but do not have sufficient particle flux to drive the reversible scavenging. As a result, the abyssal crustal Pb isotope signatures mix in laterally and dominate the deep ocean dPb isotope ratios at these stations. This comparison across stations is a beautiful illustration of how particle fluxes do drive reversible scavenging–facilitated deepening of anthropogenic dPb isotope signatures year-round, but the isotope anomaly should always be strongest at the location of current highest particle flux (assuming constant dPb isotopes in the upper ocean), as deep ocean mixing rates are sufficient to erode the deep water isotope anomaly even over the course of a year in this part of the Pacific Ocean.

In this paper, we have used Pb isotope ratios to visualize the influence of reversible scavenging in a way that has been challenging to distinguish from vertical regeneration processes previously. We showed how this reversible scavenging is responsible for injecting anthropogenic Pb into the otherwise-pristine deep oceans. We also applied a diagnostic model across the natural gradients observed in our Pacific Ocean dataset that allowed us to constrain the dominance of these reversible scavenging–associated dPb deepening events to regions of high particle flux that otherwise had strong surface-deep dPb isotope gradients. Particle veils have provided a unique opportunity to further understand the cycling of Pb in the marine environment and the role that reversible scavenging may play in the distribution of dPb and its isotopes. Aside from Pb, reversible scavenging has been described for several other trace elements but is especially crystallized here for Pb because of its short <80 y deep ocean residence time (18) and its escape from biological cycling processes such as regeneration that might otherwise obscure these scavenging signals. The study of Pb in the marine environment offers a unique opportunity to track the origin, circulation, and fate of human contamination in an ever-evolving global experiment.

Materials and Methods

The U.S. GEOTRACES program conducted the Pacific Meridional Transect (GP15) between September 18 and November 24, 2018, aboard the R/V *Revelle*, which sampled from the Alaskan shelf to Tahiti along 152°W. Seawater samples were collected using a 24-bottle trace metal clean Go-Flo rosette with an epoxy-coated aluminum frame (53). In addition, a surface "tow-fish" collected surface samples at each station and intermittently between stations.

Seawater for dPb and stable dPb isotopes was subsampled from the Go-Flo bottles and filtered at 0.2 μm with an acid-cleaned Acropak-200 filter (Pall) under HEPA-filtered air. Samples for dPb concentration analysis were filtered into acid-cleaned 250 mL Low Density PolyEthylene (LDPE) Nalgene bottles and acidified to ~0.024 M ultrapure HCl (Fisher Scientific, Optima grade). Samples for stable Pb isotope analysis were filtered into 2 L acid-cleaned High Density Polyethylene (HDPE) Nalgene bottles and acidified to ~0.012 ultrapure HCl. These seawater samples were stored for more than 4 mo. and analyzed back on land (54).

Ultrafiltration of dPb samples was also conducted to tease apart the dissolved phase into colloidal Pb (0.003 to 0.2 μm) and soluble or truly dissolved Pb (<0.003 μm ~ 10 kDa). Approximately 350 mL of dissolved seawater was ultrafiltered using cross flow filtration (<0.003 μm ~ 10 kDa) to remove the colloidal size fraction as has been successfully done in the past for iron colloids (47).

Particle samples were separated into small (1 to 51 μm) and large (>51 μm) size fractions using McLane Research in situ pumps (WTS-LV or Water Transfer System-Large Volume), which were each equipped with two 142-mm filter holders

(30, 55). One holder was loaded with a 51-μm Sefar polyester mesh followed by a pair of 0.8-μm Pall Supor polyethersulfone filters, while the other was loaded with the same polyester mesh followed by paired Whatman QMA (Quartz Microfiber -A) filters (1-μm nominal porosity).

Dissolved Pb concentration was analyzed at Texas A&M University (TAMU) using an automated, flow-injection SeaFAST pico offline ICP-MS method (54, 56). Isotope dilution was employed to quantify the dPb concentration. Once the metals were extracted, the samples were analyzed for Pb in low resolution on an Element XR High Resolution-Inductively Coupled Plasma-Mass Spectometer (HR-ICP-MS) in the TAMU R. Ken Williams Radiogenic Isotope Laboratory. At three stations, dPb was also measured at the Massachusetts Institute of Technology (MIT) using a modified isotope dilution batch method; the agreement with the TAMU data was good (*SI Appendix*, Fig. S3).

Stable dPb isotopes (^{206}Pb, ^{207}Pb, ^{208}Pb) were measured at MIT by employing an updated method modified from previous work (57–59). Lead is extracted from the seawater using $Mg(OH)_2$ coprecipitation followed by redissolution and adsorption onto Nobias PA1 chelating resin (59). The adsorbed metals are then dissolved in nitric and passed through a solid-phase extraction column of AG1-X8 resin. Once through the column, the samples are analyzed on a GV/Micromass IsoProbe MultiCollector-Inductively Couple Plasma-Mass Spectrometer (MC-ICP-MS) with Faraday cups used for ^{206}Pb, ^{207}Pb, and ^{208}Pb.

PIC was measured via coulometry from filters from the QMA-equipped filter holders. SPM was estimated as the chemical dry weight of the major particulate components [particulate organic matter, opal, $CaCO_3$, lithogenic material, and Fe and Mn (oxyhydroxides), which were each measured separately (30, 55)]. Leachable lead in the small size fraction (1 to 51 μm) was measured using a weak acid leach targeting the labile fraction of various metals (60). In short, partial Supor filters (1/16) were leached in a solution of 25% acetic acid and 0.2 M hydroxylamine hydrochloride with gentle heating to isolate the labile fraction. After cooling, the samples were centrifuged and the supernatant was extracted, dried down, and digested with HNO_3. The resulting leach solution was diluted in a solution with 5% HNO_3 and 1 ppb indium and was analyzed by using an Element XR HR-ICP-MS in the University of California Santa Cruz (UCSC) Plasma Analytical Facility.

Data, Materials, and Software Availability. All study data are included in the article and/or *SI Appendix*.

ACKNOWLEDGMENTS. This work was made possible by the tireless efforts of the U.S. GEOTRACES GP15 Chief Scientists and "super-tech" team who subsampled all trace metal samples (Dr. Laramie Jensen & Brent Summers), hydrographic samples (Colette Kelly & Marty Fleisher), and surface tow-fish samples (Sveinn Einarsson & Kyle McQuiggan). We thank Richard Rosas and Dr. Christina Wiederwohl for their help with figure generation in Matlab. We also appreciate assistance from Rick Kayser while analyzing Pb isotopes. Allison Laubach and Dr. Jong-Mi Lee measured total particulate trace metals used for the MnOx and SPM determinations; Nicholas Carracino and Sophie Rojas measured particulate organic carbon used in SPM determinations. Lastly, we would like to thank the captain and crew of the R/V *Roger Revelle*. This work was funded by NSF grants OCE-1737167 (J.N.F.), OCE-1736996 (E.A.B.), OCE-1736601, and OCE-1657781 (P.J.L.). Additionally, this work was funded by an NSF Graduate Research Fellowship Program (GRFP) to N.T.L., V.J.A., and K.M., as well as the UC Cota-Robles Fellowship to V.J.A.

Author affiliations: [a]Department of Oceanography, Texas A&M University, College Station, TX 77840; [b]Department of Earth, Atmospheric, and Planetary Sciences, Massachusetts Institute of Technology, Cambridge, MA 02139; [c]State Key Laboratory of Estuarine and Coastal Research, East China Normal University, Shanghai 200241, China; and [d]Department of Ocean Sciences, University of California Santa Cruz, Santa Cruz, CA 95064

1. H. Craig, A scavenging model for trace elements in the deep sea. *Earth Planetary Sci. Lett.* **23**, 149–159 (1974).
2. L. Balistrieri, P. Brewer, J. Murray, Scavenging residence times of trace metals and surface chemistry of sinking particles in the deep ocean. *Deep Sea Res. Part A. Oceanogr. Res. Pap.* **28**, 101–121 (1981).
3. M. P. Bacon, R. F. Anderson, Distribution of thorium isotopes between dissolved and particulate forms in the deep sea. *J. Geophys. Res. Oceans* **87**, 2045–2056 (1982).
4. J. Wu, R. Rember, M. Jin, E. A. Boyle, A. R. Flegal, Isotopic evidence for the source of lead in the North Pacific abyssal water. *Geochim. Cosmochim. Acta* **74**, 4629–4638 (2010).
5. R. M. Sherrell, E. A. Boyle, B. Hamelin, Isotopic equilibration between dissolved and suspended particulate lead in the Atlantic Ocean: Evidence from 210Pb and stable Pb isotopes. *J. Geophys. Res. Oceans* **97**, 11257–11268 (1992).
6. S. Little, D. Vance, M. Siddall, E. Gasson, A modeling assessment of the role of reversible scavenging in controlling oceanic dissolved Cu and Zn distributions. *Global Biogeochem. Cycles* **27**, 780–791 (2013).
7. J. N. Fitzsimmons *et al.*, Iron persistence in a distal hydrothermal plume supported by dissolved–particulate exchange. *Nat. Geosci.* **10**, 195–201 (2017).
8. S. Roshan, T. DeVries, J. Wu, S. John, T. Weber, Reversible scavenging traps hydrothermal iron in the deep ocean. *Earth Planetary Sci. Lett.* **542**, 116297 (2020).
9. T. M. Conway, S. G. John, The cycling of iron, zinc and cadmium in the North East Pacific Ocean-Insights from stable isotopes. *Geochim. Cosmochim. Acta* **164**, 262–283 (2015).
10. R. K. Seth John *et al.*, The biogeochemical cycling of oceanic nickel cycling. *Nat. Geosci.* **15**, 906–912 (2022).
11. T. Weber, S. John, A. Tagliabue, T. DeVries, Biological uptake and reversible scavenging of zinc in the global ocean. *Science* **361**, 72–76 (2018).
12. C. Richon, A. Tagliabue, Insights into the major processes driving the global distribution of copper in the ocean from a global model. *Global Biogeochem. Cycles* **33**, 1594–1610 (2019).
13. J.-M. Lee *et al.*, Impact of anthropogenic Pb and ocean circulation on the recent distribution of Pb isotopes in the Indian Ocean. *Geochim. Cosmochim. Acta* **170**, 126–144 (2015).
14. S. Lee *et al.*, Characteristics of elemental and Pb isotopic compositions in aerosols (PM10-2.5) at the Ieodo Ocean Research Station in the East China Sea. *Environ. Pollut.* **231**, 154–164 (2017).
15. R. Khondoker *et al.*, New constraints on elemental and Pb and Nd isotope compositions of South American and Southern African aerosol sources to the South Atlantic Ocean. *Geochemistry* **78**, 372–384 (2018).
16. P. Pinedo-González *et al.*, Anthropogenic Asian aerosols provide Fe to the North Pacific Ocean. *Proc. Natl. Acad. Sci. U.S.A.* **117**, 27862–27868 (2020).
17. E. A. Boyle *et al.*, Anthropogenic lead emissions in the ocean: The evolving global experiment. *Oceanography* **27**, 69–75 (2014).
18. A. Flegal, C. Patterson, Vertical concentration profiles of lead in the Central Pacific at 15 N and 20 S. *Earth Planetary Sci. Lett.* **64**, 19–32 (1983).
19. B. K. Schaule, C. C. Patterson, Lead concentrations in the northeast Pacific: Evidence for global anthropogenic perturbations. *Earth Planetary Sci. Lett.* **54**, 97–116 (1981).
20. E. A. Boyle, B. A. Bergquist, R. A. Kayser, N. Mahowald, Iron, manganese, and lead at Hawaii Ocean Time-series station ALOHA: Temporal variability and an intermediate water hydrothermal plume. *Geochim. Cosmochim. Acta* **69**, 933–952 (2005).
21. C. Gallon *et al.*, Asian industrial lead inputs to the North Pacific evidenced by lead concentrations and isotopic compositions in surface waters and aerosols. *Environ. Sci. Technol.* **45**, 9874–9882 (2011).
22. A. Flegal, B. Schaule, C. Patterson, Stable isotopic ratios of lead in surface waters of the Central Pacific. *Marine chem.* **14**, 281–287 (1984).
23. C. M. Zurbrick, C. Gallon, A. R. Flegal, Historic and industrial lead within the Northwest Pacific Ocean evidenced by lead isotopes in seawater. *Environ. Sci. Technol.* **51**, 1203–1212 (2017).
24. H. Cheng, Y. Hu, Lead (Pb) isotopic fingerprinting and its applications in lead pollution studies in China: A review. *Environ. Pollution* **158**, 1134–1146 (2010).
25. E. A. Boyle *et al.*, Lead and lead isotopes in the US GEOTRACES East Pacific zonal transect (GEOTRACES GP16). *Marine Chem.* **227**, 103892 (2020).
26. A. Bollhöfer, K. Rosman, Isotopic source signatures for atmospheric lead: The Northern Hemisphere. *Geochim. Cosmochim. Acta* **65**, 1727–1740 (2001).
27. M. Chen *et al.*, Lead isotope exchange between dissolved and fluvial particulate matter: A laboratory study from the Johor River estuary. *Phil. Trans. R. Soc. A* **374**, 20160054 (2016).
28. R. Kiko *et al.*, Biological and physical influences on marine snowfall at the equator. *Nat. Geosci.* **10**, 852–858 (2017).
29. L. Juranek *et al.*, Biological production in the NE Pacific and its influence on air-sea CO2 flux: Evidence from dissolved oxygen isotopes and O2/Ar. *J. Geophys. Res. Oceans* **117**, C00F450 (2012).
30. J. K. B. Bishop *et al.*, Transmitted cross-polarized light detection of particulate inorganic carbon concentrations and fluxes in the ocean water column: Ships to ARGO floats. *Front. Remote Sensing* **3**, 837938 (2022).
31. L. Zheng *et al.*, Distinct basin-scale-distributions of aluminum, manganese, cobalt, and lead in the North Pacific Ocean. *Geochim. Cosmochim. Acta* **254**, 102–121 (2019).
32. S. Jiang, J. Zhang, H. Zhou, Y. Xue, W. Zheng, Concentration of dissolved lead in the upper Northwestern Pacific Ocean. *Chem. Geol.* **577**, 120275 (2021).
33. J. A. Kenyon, "Anthropogenic and natural radioisotopes as tracers for contaminant sources and particulate fluxes," PhD thesis, Massachusetts Institute of Technology and Woods Hole Oceanographic Institution, Cambridge, MA (2022).
34. C. T. Hayes *et al.*, Intensity of Th and Pa scavenging partitioned by particle chemistry in the North Atlantic Ocean. *Marine Chem.* **170**, 49–60 (2015).
35. Y. Xiang, P. J. Lam, A. B. Burd, C. T. Hayes, Estimating mass flux from size-fractionated filtered particles: Insights into controls on sinking velocities and mass fluxes in recent US GEOTRACES cruises. *Global Biogeochem. Cycles* **36**, e2021GB007292 (2022).
36. B. D. Honeyman, L. S. Balistrieri, J. W. Murray, Oceanic trace metal scavenging: The importance of particle concentration. *Deep Sea Res. Part A Oceanogr. Res. Pap.* **35**, 227–246 (1988).
37. S. Bradley Moran, K. O. Buesseler, Size-fractionated 234Th in continental shelf waters off New England: Implications for the role of colloids in oceanic trace metal scavenging. *J. Marine Res.* **51**, 893–922 (1993).
38. B. Honeyman, P. Santschi, A Brownian-pumping model for oceanic trace metal scavenging: Evidence from Th isotopes. *J. Marine Res.* **47**, 951–992 (1989).
39. P. Lerner, O. Marchal, P. J. Lam, K. Buesseler, M. Charette, Kinetics of thorium and particle cycling along the US GEOTRACES North Atlantic Transect. *Deep Sea Res. Part I Oceanogr. Res. Pap.* **125**, 106–128 (2017).
40. C. J. Roach, D. Balwada, K. Speer, Global observations of horizontal mixing from Argo float and surface drifter trajectories. *J. Geophys. Res. Oceans* **123**, 4560–4575 (2018).

41. J. W. Campbell, T. Aarup, New production in the North Atlantic derived from seasonal patterns of surface chlorophyll. *Deep Sea Res. Part A Oceanogr. Res. Pap.* **39**, 1669–1694 (1992).
42. C. M. Zurbrick *et al.*, Dissolved Pb and Pb isotopes in the North Atlantic from the GEOVIDE transect (GEOTRACES GA-01) and their decadal evolution. *Biogeosciences* **15**, 4995–5014 (2018).
43. A. E. Noble *et al.*, Dynamic variability of dissolved Pb and Pb isotope composition from the US North Atlantic GEOTRACES transect. *Deep Sea Res. Part II Top. Stud. Oceanogr.* **116**, 208–225 (2015).
44. B. M. Tebo *et al.*, Biogenic manganese oxides: Properties and mechanisms of formation. *Annu. Rev. Earth Planet. Sci.* **32**, 287–328 (2004).
45. W. Bam *et al.*, Variability in 210Pb and 210Po partition coefficients (Kd) along the US GEOTRACES Arctic transect. *Marine Chem.* **219**, 103749 (2020).
46. Y. Tang, G. Stewart, P. J. Lam, S. Rigaud, T. Church, The influence of particle concentration and composition on the fractionation of 210Po and 210Pb along the North Atlantic GEOTRACES transect GA03. *Deep Sea Res. Part I Oceanogr. Res. Pap.* **128**, 42–54 (2017).
47. J. N. Fitzsimmons, E. A. Boyle, Assessment and comparison of Anopore and cross flow filtration methods for the determination of dissolved iron size fractionation into soluble and colloidal phases in seawater. *Limnol. Oceanogr. Methods* **12**, 246–263 (2014).
48. J. J. Polovina, G. T. Mitchum, G. T. Evans, Decadal and basin-scale variation in mixed layer depth and the impact on biological production in the Central and North Pacific, 1960–88. *Deep Sea Res. Part I Oceanogr. Res. Pap.* **42**, 1701–1716 (1995).
49. R. Francois, S. Honjo, R. Krishfield, S. Manganini, Factors controlling the flux of organic carbon to the bathypelagic zone of the ocean. *Global Biogeochem. Cycles* **16**, 34-31–34-20 (2002).
50. E. Howard, S. Emerson, S. Bushinsky, C. Stump, The role of net community production in air-sea carbon fluxes at the North Pacific subarctic-subtropical boundary region. *Limnol. Oceanogr.* **55**, 2585–2596 (2010).
51. C. L. Follett, S. Dutkiewicz, G. Forget, B. Cael, M. J. Follows, Moving ecological and biogeochemical transitions across the North Pacific. *Limnol. Oceanogr.* **66**, 2442–2454 (2021).
52. J. J. Polovina, E. A. Howell, D. R. Kobayashi, M. P. Seki, The transition zone chlorophyll front updated: Advances from a decade of research. *Prog. Oceanogr.* **150**, 79–85 (2017).
53. G. A. Cutter, K. W. Bruland, Rapid and noncontaminating sampling system for trace elements in global ocean surveys. *Limnol. Oceanogr. Methods* **10**, 425–436 (2012).
54. L. Jensen, N. Wyatt, W. Landing, J. Fitzsimmons, Assessment of the stability, sorption, and exchangeability of marine dissolved and colloidal metals. *Marine Chem.* **220**, 103754 (2020).
55. Y. Xiang, P. J. Lam, Size-fractionated compositions of marine suspended particles in the Western Arctic Ocean: Lateral and vertical sources. *J. Geophys. Res. Oceans* **125**, e2020JC016144 (2020).
56. M. Lagerström *et al.*, Automated on-line flow-injection ICP-MS determination of trace metals (Mn, Fe Co, Ni, Cu and Zn) in open ocean seawater: Application to the GEOTRACES program. *Marine Chem.* **155**, 71–80 (2013).
57. E. A. Boyle *et al.*, GEOTRACES IC1 (BATS) contamination-prone trace element isotopes Cd, Fe, Pb, Zn, Cu, and Mo intercalibration. *Limnol. Oceanogr. Methods* **10**, 653–665 (2012).
58. M. K. Reuer, E. A. Boyle, B. C. Grant, Lead isotope analysis of marine carbonates and seawater by multiple collector ICP-MS. *Chem. Geol.* **200**, 137–153 (2003).
59. E. Boyle, An improved low-blank method for the preconcentration of Pb isotopes from seawater. *Goldschmidt* (2021), Honolulu, HI.
60. C. J. Berger, S. M. Lippiatt, M. G. Lawrence, K. W. Bruland, Application of a chemical leach technique for estimating labile particulate aluminum, iron, and manganese in the Columbia River plume and coastal waters off Oregon and Washington. *J. Geophys. Res. Oceans* **113** (2008).